



# Dynamic pressure evolution within the 18 May 1980 Mount St. Helens pyroclastic density current: evidence from tree damage

Nicole K. Guinn<sup>1</sup> · James E. Gardner<sup>1</sup> · Mark A. Helper<sup>1</sup>

Received: 26 October 2021 / Accepted: 25 February 2022 / Published online: 18 March 2022  
© The Author(s) 2022

## Abstract

The effects of pyroclastic density currents (PDCs) can be devastating, so understanding their internal dynamics and evolution is important for hazard assessment. We use damaged trees located around Mount St. Helens (USA) as proxy for the dynamic pressure ( $P_{dyn}$ ) of the PDC erupted on 18 May 1980. We recorded the location, distribution, and foliage preservation of damaged trees within the medial and distal parts of the devastated forest. Sub-meter resolution aerial photographs from a month after the eruption allow distinction between standing trees that retained foliage from those that were stripped. Heights of standing trees were estimated from the measured lengths of their shadows. The number of standing trees was counted within defined areas along the propagation paths of PDCs. From the measured tree heights, we estimated tree toppling stresses from  $P_{dyn}$ . Overall,  $P_{dyn}$  of the PDC head within the medial to distal portions of the blowdown zone ranged from 10 to 35 kPa.  $P_{dyn}$  likely waned with distance, as shown by the increased number of standing trees in the outer parts of the devastated area. In addition, we find clusters of standing trees on the lee sides of some hills. We propose that these clusters survived because they were primarily impacted by lower dynamic pressures extant within the PDC body, with foliage retention or stripping as a function of the  $P_{dyn}$  evolution in the PDC body. We estimate that  $P_{dyn}$  of the body was less than the estimated maximum  $P_{dyn}$  of the PDC head by  $12 \pm 4$  kPa.

**Keywords** Pyroclastic density current · Dynamic pressure · Aerial photography · Mount St. Helens · Tree damage · Volcanic hazards

## Introduction

Pyroclastic density currents (PDCs) are hot, gaseous, tephra-laden currents that move at high speeds as a result of the effect of gravity (Baxter 1990; Auker et al. 2013; Baxter et al. 2017). These currents follow topography because they are denser than the atmosphere (Druitt 1998; Branney and Kokelaar 2002; Dufek et al. 2015). Few humans or structures can survive these devastating flows (e.g., Blong 1984; Baxter 1990; Baxter et al. 1998; Valentine 1998; Auker et al. 2013), making investigations of their mechanics and evolution a critical topic for hazard assessment. Much of the

damage caused by a PDC results from the lateral force it exerts, which is expressed as dynamic pressure ( $P_{dyn}$ ):

$$P_{dyn} = \frac{1}{2} \rho v^2 \quad (1)$$

where  $\rho$  is bulk flow density and  $v$  is velocity (Valentine 1998; Baxter et al. 2005; Jenkins et al. 2013). PDC is an all-encompassing term that includes end members such as a dense pyroclastic flow and a dilute pyroclastic surge (Branney and Kokelaar 2002; Andrews and Manga 2012). PDCs can also be stratified with a denser regime below a dilute regime (Branney and Kokelaar 2002; Gardner et al. 2007; Andrews and Manga 2012).

Measuring the in situ  $P_{dyn}$  of a PDC is too hazardous, and so, alternative methods are necessary. Some studies have used tree damage as a proxy (Valentine 1998; Clarke and Voight 2000; Kelfoun et al. 2000; Baxter et al. 2005; Pitarri et al. 2007; Jenkins et al. 2013; Brand et al. 2014). For example, Brand et al. (2014) used the lengths of downed trees to infer a range of 12–35 kPa at 0.9 km from the source

---

Editorial responsibility: L. Pioli

---

✉ Nicole K. Guinn  
nkg425@utexas.edu

<sup>1</sup> Department of Geological Sciences, Jackson School of Geosciences, The University of Texas at Austin, Austin, TX 78712-0254, USA

at Maungataketake tuff ring (Auckland Volcanic Field, New Zealand), and Clarke and Voight (2000) used a downed tree to estimate  $P_{dyn} = 39.7$  kPa at 8 km from Mount St. Helens (1980 directed blast surge). Jenkins et al. (2013) used tree damage in conjunction with damage to other objects and buildings to estimate  $P_{dyn}$  of more than 15 kPa at 6 km from the 2010 dome collapse at Merapi (Indonesia). Although such studies provide important constraints on  $P_{dyn}$ , most focused on single trees and thus do not provide information on how  $P_{dyn}$  evolves in a moving PDC. Kelfoun et al. (2000) mapped out the dynamics of PDCs using zones of tree damage, but did not quantify how  $P_{dyn}$  varied. Numerical models that allow constraining flow variables such as  $P_{dyn}$  have also been used to improve hazard maps and influence assessments of structural vulnerability within PDC emplacement zones (Esposti Ongaro et al. 2002, 2011; Doronzo et al. 2011; Roche et al. 2013), being useful to understand time and distance-dependent variations of this parameter.

In order to better understand the spatial and temporal evolution of  $P_{dyn}$ , we re-evaluated tree damage throughout the  $\sim 600$ -km $^2$  forest that was nearly leveled by the PDC erupted on the morning of 18 May 1980 from Mount St. Helens (c.f. Rosenfeld 1980; Hoblitt et al. 1981; Moore and Sisson 1981; Snellgrove et al. 1983). This eruption was triggered by a 5.1 magnitude earthquake that caused the northern flank to fail as a landslide and expose the growing cryptodome. The explosion of the cryptodome erupted the laterally directed PDC that lasted 4–5 min (Christiansen and Peterson 1981; Hoblitt 2000; Branney and Kokelaar 2002; Gardner et al. 2017). From proximal to distal zones, the devastated forest is comprised of zones of complete tree removal, of mainly leveled trees (the blowdown zone), and of standing burned trees (the scorched zone) (Figs. 1a and 2a; Rosenfeld, 1980; Hoblitt et al., 1981; Moore and Sisson, 1981; Waitt, 1981). Clusters of partially damaged trees were left standing on the lee sides of hills or topographic drop-offs in the blowdown zone (Fig. 2b; see Plate 1 in Lipman Mullineaux, 1981; Gardner et al. 2018). In addition, damaged solitary trees were left standing throughout the blowdown zone, most of which were partially broken and stripped of vegetation (Snellgrove et al. 1983). Extending the work of Gardner et al. (2018), here we systematically mapped and investigated tree damage to infer the evolution of  $P_{dyn}$  with distance and direction from the source. We find that the  $P_{dyn}$  of the PDC head likely decreased with distance from the volcano and that standing tree clusters were impacted by lower  $P_{dyn}$  within the PDC body.

## Methods

We located, mapped, and measured characteristics of standing and downed trees within the medial (5–15 km) and distal portions (15–30 km) of the blowdown zone.

Single frame, 1:29,857, 0.8-m-resolution, color-infrared aerial images acquired on 19 June 1980 by the US Geological Survey were georeferenced to the blowdown zone. A 1/3 arc-sec ( $\sim 10$  m) resolution digital elevation model (DEM; <https://ned.usgs.gov>) of the topography immediately after the eruption was used to derive slope, aspect, and hillshade rasters using ArcGIS (<https://www.esri.com/en-us/arcgis/about-arcgis/overview>). The vertical resolution of the DEM at 95% confidence interval is 3.04 m.

Standing trees were recognized and characterized by the shadows they cast and by their proximity to other standing tree shadows. Nearly linear tree shadows are produced by standing trees without foliage (Fig. 3a). Shadows that are irregular and more rounded are from standing trees that retained foliage (Fig. 3b), as evidenced by shadows of such trees in the scorched zone (Figs. 2a and 3c; Rosenfeld 1980; Tilling et al. 1990). We further categorized standing trees as either solitary or clustered. Clusters of standing trees are defined in areas with ten or more closely spaced (within 5 m) linear or irregular tree shadows (Figs. 2b and 3b). The outlines of standing tree clusters were digitized to create polygons whose areas were calculated within ArcGIS. Cluster areas have uncertainties that range from 0.1 to 3% for the largest and smallest clusters, respectively. Solitary standing trees are defined by shadows spaced more than 5 m from other tree shadows (Fig. 3c). All standing tree shadows were measured from the digitized distance between their shadow ends. The lack of obvious solitary tree shadows in the northwest portion of the blowdown zone prevented study there due to recent logging, even though tree clusters are visible (Gardner et al. 2018).

Felled trees were identified by their linear aspect and characteristic albedo (Fig. 3c). Their lengths were measured as the digitized distance between the two ends of a tree. Only solitary, felled tree lengths were measured because the energy needed to topple trees may be reduced when trees fall in groups (Clarke and Voight 2000). The length of a felled tree is assumed equal to its height when standing.

Heights of standing trees cannot be directly measured from the aerial photographs. Instead, the height ( $z$ ) of a vertical tree was derived from the length of its shadow on horizontal ground ( $b$ ) using the following:

$$z = b \times \tan\theta \quad (2)$$

where  $\theta$  is the solar elevation (Fig. 4a). Solar elevation ( $\theta$ ) was derived from an interactive sun path chart web application (<http://solardat.uoregon.edu/SunChartProgram.html>) that required only location coordinates and solar azimuth for the day the aerial photographs were acquired (19 June 1980). Solar azimuth is the same as the

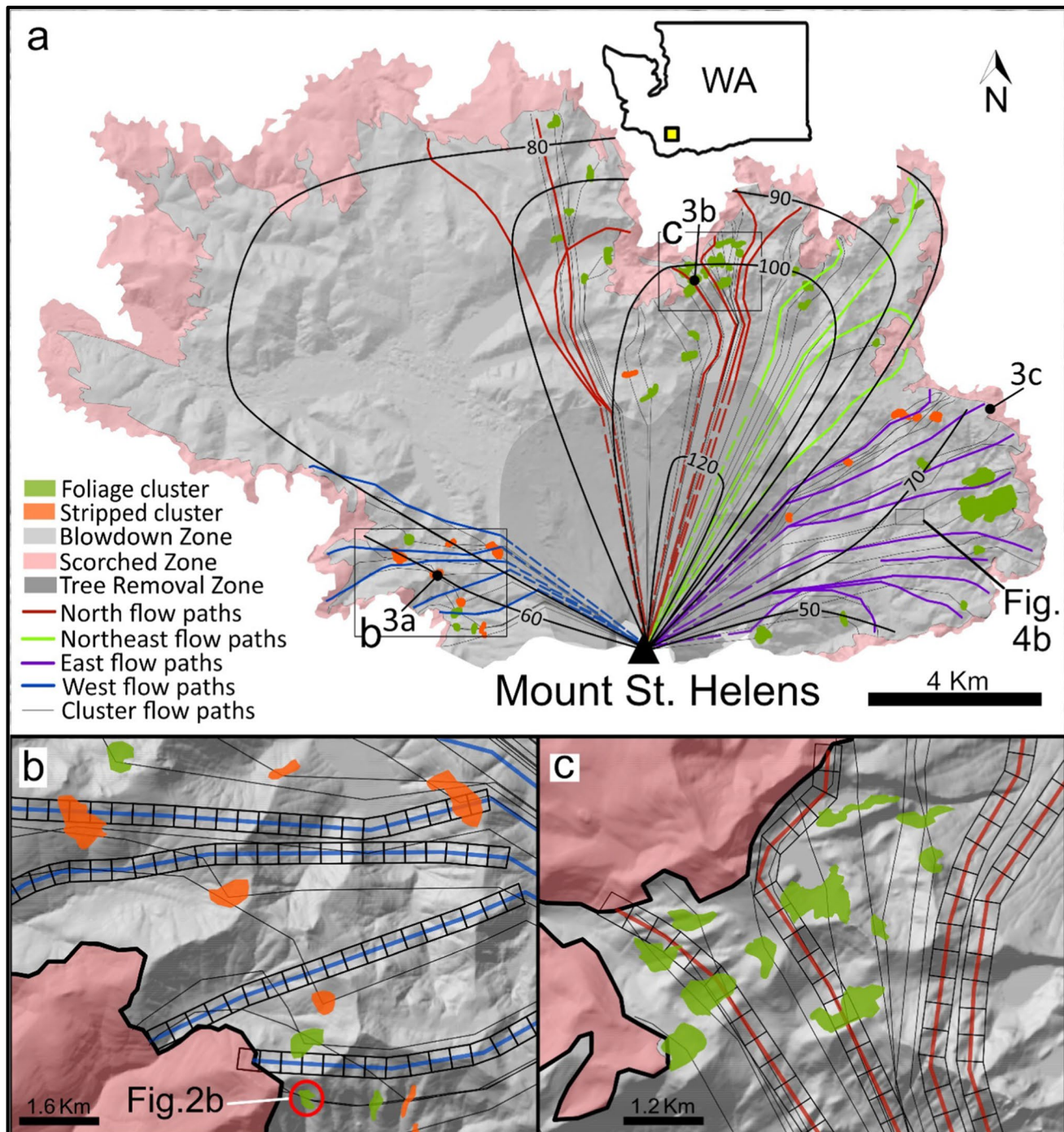


**Fig. 1** **a** Shaded relief map of the area devastated by the eruption, showing all standing tree clusters, PDC flow paths, and locations of Fig. **1b** and **c**. Inset map shows the location (yellow box) of Fig. **1a** in Washington state, USA. The blowdown zone contains standing tree clusters, solitary standing trees, and felled trees. The scorched zone contains only standing, burned trees. Outside the scorched zone are standing, living trees. Flow paths near standing solitary trees in the blowdown zone are separated into directional zones by color. Three labeled black dots show locations of Fig. **3a**, **b**, and **c**. Thicker black lines are velocity contours for the PDC head in meters per second, derived from the 30-s interval isochron map of Moore and Rice

(1984). Velocity estimates were contoured at 10 m/s intervals. Location of Fig. **4b** topographic profile shown in lower right and location of Fig. **2b** photograph in the lower left. **b** Shaded relief map of a portion of the western side of the blowdown zone, where many of the stripped tree clusters are located. Thin black lines are flow paths that intersect standing tree clusters. Boxes centered on west flow paths (blue) show  $200 \times 200$  m areas used to calculate solitary standing tree densities. Location of Fig. **2b** is labeled. **c** Shaded relief map of a portion of the northern edge of the blowdown zone, where standing tree clusters that retained foliage were present

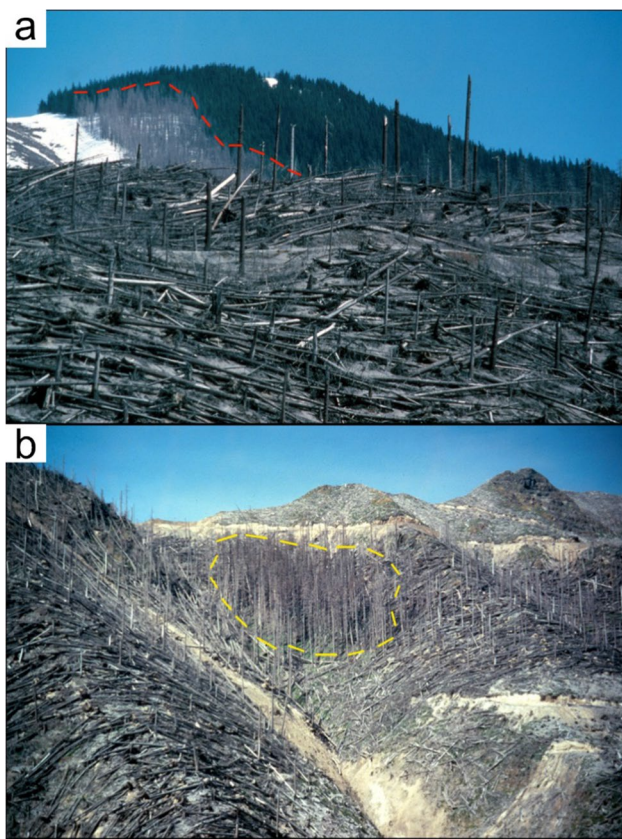


**Fig. 2** **a** Stripped, solitary trees are left standing in the blowdown zone in the foreground. Some standing trees appear much shorter than others, including the felled trees. Felled trees toppled by the PDC are also stripped, with root balls aligned toward the oncoming PDC. The red dashed line is the outer edge of the scorch zone, separating scorched, standing trees from undamaged trees in the background. US Geological Survey/photo by Lyn Topinka, 1982. **b** Foliage cluster (encircled by yellow dashed line) of standing trees in the western area of the blowdown zone (location indicated in Fig. 1b). Trees in the cluster have burned foliage and are situated on the lee side of a hill. Surrounding trees were felled by the PDC. US Geological Survey/photo by Lyn Topinka

shadow azimuth ( $\gamma$ ) of a standing tree in the georeferenced photographs, as determined with software tools after the shadow is digitized. Most, if not all, trees are on sloping ground, so tree shadow lengths ( $l$ ) can be longer or shorter in aerial photographs compared to *b*. Tree shadow lengths ( $l$ ) were corrected for slope and converted to a horizontal shadow length ( $b$ ) by the following:

$$b = \frac{l \times \sin(\theta - \alpha)}{\sin(180 - \theta)} \quad (3)$$

where  $\alpha$  is the slope of the ground on which a shadow was cast (Fig. 4a). Our 10-m-resolution, DEM-derived slope raster, however, contains pixels of maximum slope ( $\delta$ ), yet individual tree shadows are rarely pointed directly

downhill or uphill;  $\alpha$  is thus not equal to  $\delta$ . We estimated  $\alpha$  from  $\delta$  using the following:

$$\alpha = \arctan [\tan \delta \times \sin(\gamma - \beta)] \quad (4)$$

where  $\beta$  is the right-hand-rule strike (azimuth) of the hill, found by subtracting  $90^\circ$  from the ground aspect azimuth available from a 10-m-resolution aspect raster. Values for  $\delta$  and  $\beta$  were measured within 5 m of each tree shadow and averaged over the length of the shadow.

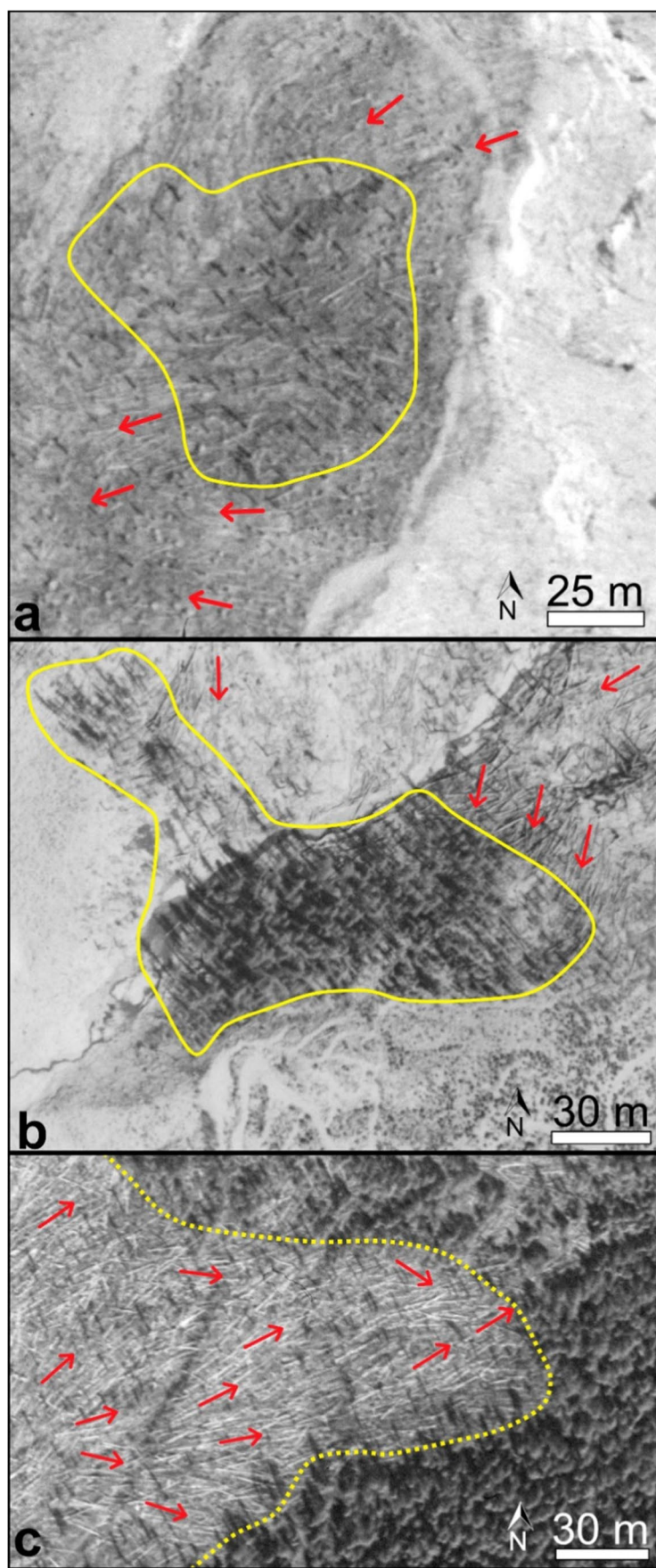
We measured only those shadows longer than 10 m in order to intersect at least two slope and aspect raster pixels. All easily identified shadows longer than 10 m in every standing tree cluster and solitary tree along the gridded flow paths (see below) were measured (Online Resource 1). To better facilitate comparisons, only felled trees longer than 10 m were measured.

Uncertainty on lengths of felled tree heights is  $\pm 0.8$  m, as governed by the resolution of the aerial photographs. The uncertainty of calculated standing tree height is greater, because of the relatively coarse 10-m-resolution DEM used to measure slope and aspect. To evaluate this error, we compared a subset of the results to those derived using a more recent (2 November 2002) 3-m-resolution DEM that covers a fraction of the blowdown zone. Standing tree heights from the two DEMs agree, on average, to within 3 m with no indication of systematic error. Height uncertainties associated solely with the 0.8-m resolution of shadow length ( $l$ ) measurements, when propagated through Eq. (4), are approximately 2 m, independent of slope and aspect. Combined, these results suggest that the total uncertainty is  $\pm 5$  m.

The above tree characteristics were measured and recorded with distance from the source along PDC flow paths. Those paths were mapped throughout most of the blowdown zone by following the alignment of felled trees. Flow path lengths have a nominal uncertainty of 0.8 m, i.e., the resolution of the aerial photographs. The most proximal portions of the PDC flow paths cannot be mapped this way because they traverse the zone where all trees were removed (Fig. 1a; Rosenfeld 1980; Hoblitt et al. 1981; Moore and Sisson 1981; Waitt 1981). Flow paths extrapolated through this region were mapped by finding the shortest straight line connecting the center of Mount St. Helens crater to a path outside the tree removal zone (Fig. 1a). To facilitate comparison of distances among paths of varied lengths, distances along all paths were normalized to the map (2D) length of each path. Flow paths tracked by the orientation of felled trees terminate at the edge of the blowdown zone.

Two groups of PDC flow paths were mapped (Fig. 1a). The first group ( $n = 93$ ) is composed of paths extended from Mount St. Helens crater to standing tree clusters and

**Fig. 3** Example aerial photographs with tree shadows. Red arrows point in the direction the PDC flowed, as determined by the orientation of felled trees. The illumination producing the tree shadows is from the southeast. Locations of aerial photos are shown in Fig. 1a. **a** A stripped cluster of standing trees is encompassed by the yellow line. Shadows are distinctly linear. **b** A cluster of standing trees with foliage, encompassed by the yellow line. Shadows have an irregular shape. **c** Solitary, standing trees intermixing with felled trees. Dotted yellow line separates the blowdown zone from the scorched zone



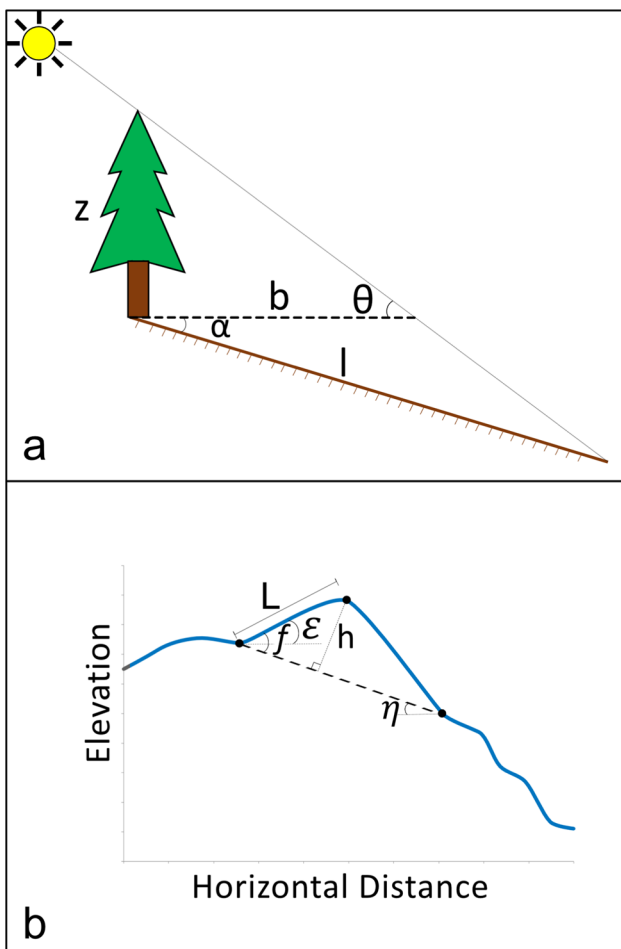


**Fig. 4** **a** The method used to calculate tree height ( $z$ ) from tree shadow length ( $l$ ). Other parameters are tree shadow length projected onto a horizontal plane ( $b$ ), the apparent slope ( $\alpha$ ), and the solar elevation ( $\theta$ ). **b** Schematic of a topographic profile that shows the parameters used to find the foreslope angle ( $f$ ) and hill height ( $h$ ) of a localized hill. The location of this topographic profile is shown in Fig. 1

then beyond to the edge of the blowdown zone. The second group ( $n=25$ ; Online Resource 2) of paths extend from the crater outward toward areas of solitary standing trees and beyond to the edge of the blowdown zone, allowing solitary standing and felled trees to be counted and measured at similar distances from the volcano. Solitary standing tree densities (trees/m<sup>2</sup>) were counted within 200 × 200 m gridded areas centered along each of the 25 group 2 flow paths (Fig. 1b, c).

In some cases, flow paths of the two groups cross (Fig. 1a–c). Overlapping lobes of the PDC felled and oriented trees in varying directions such that in these cases no direction characterizes uniquely the PDC flow path. There is no way to tell if flow paths truly crossed or if PDC lobes instead deflected one another.

Both groups of flow paths were used to derive the velocity of the PDC by georeferencing an isochron map from Moore and Rice (1984) (Fig. 1a). The isochron map used classified satellite imagery to map the front of the PDC at 30-s intervals. Distances between isochrons along flow paths were measured, providing an estimate of the velocity of the PDC at both solitary standing trees and tree clusters.

Hill slopes and heights were measured along flow paths that intersected standing tree clusters from DEM-derived, 1-km-long topographic profiles over a distance of 500-m upstream and downstream of each standing tree cluster (Online Resource 3). Locations and elevations along the topographic profiles of the initial inflection point, crest, and last inflection point of the hill were collected (Fig. 4b). The slope of the hillside facing the approaching PDC, referred to as the foreslope angle ( $f$ ; Fig. 4b), is the sum of the angle between the horizontal plane(s) and the topography of the localized hill ( $\epsilon$ ) and the angle created by a theoretical baseline connecting the upstream and downstream inflection points with the horizontal plane ( $\eta$ , Fig. 4b). The crest of the hill upstream of a tree cluster was identified by a change in slope. The inflection points upstream of the crest and downstream of the standing tree cluster were identified as the starting and ending locations of the hill, respectively. Hill height ( $h$ ) was defined as the difference in elevation between the crest and the baseline between the beginning and bottom of the hill (Fig. 4b). Hill height is measured perpendicular to the baseline:

$$h = L \times \sin(f) \quad (5)$$

where  $L$  is the length of the stoss side of the hill (Fig. 4b). Hill height uncertainty, governed by the vertical resolution of the DEM, is about 3 m.

## Results

A total of 1271 solitary, standing trees taller than 10 m were measured (Online Resource 1). Fewer than 2% of those occurred on slopes steeper than 30° that faced the oncoming PDC, and only 7% were on slopes steeper than 30° that faced away from the moving PDC. Towards the east and west, standing trees first appear at ~40–45% of the runout, and the number left standing increased from ~200 to as much as ~600 trees/km<sup>2</sup> after ~70–80% of runout (Fig. 5a, d). The heights of those left standing tended to be taller farther away from the volcano, reaching as tall as ~50–60 m at the end of runout (Fig. 6). To the north and northeast, standing trees were found only after 80–90% of runout, and their number densities increased greatly from ~100 to ~1000 trees/km<sup>2</sup> in the last 10% runout (Fig. 5b, c).

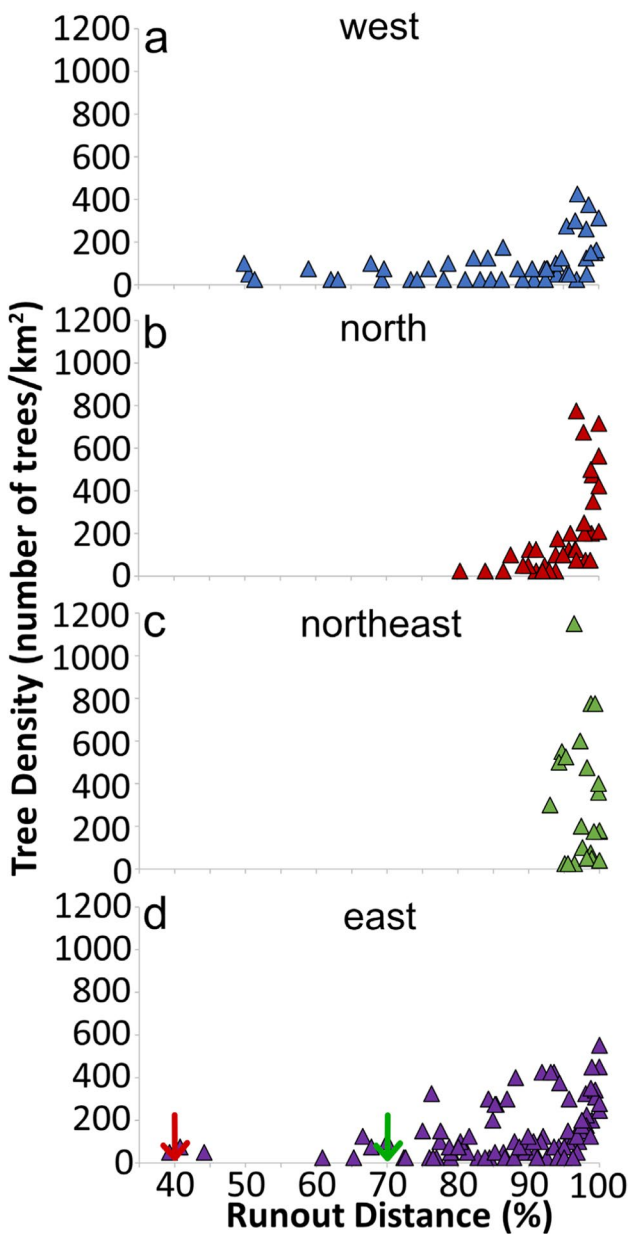


**Fig. 5** Standing tree density (number of trees/km<sup>2</sup>) as a function of normalized runout distance of the 18 May 1980 PDC. Symbol colors match the flow path coloring in Fig. 1. Standing tree densities are broken out by direction for the **a** west, **b** north, **c** northeast, and **d** east sides of the blowdown zone. The red arrow in **d** designates where stripped standing tree clusters are first noticeable; the green arrow designates where standing tree clusters that retained foliage are first visible for the east side of the blowdown zone only. Uncertainties in densities and distance are smaller than symbols

The length of felled trees increases with runout distance in all directions, except to the northeast (Fig. 6). In the northeast and east, trees that were felled were on average ~5–9 m shorter than those left standing, whereas to the west and north, heights of standing trees and lengths of felled trees are similar (Table 1).

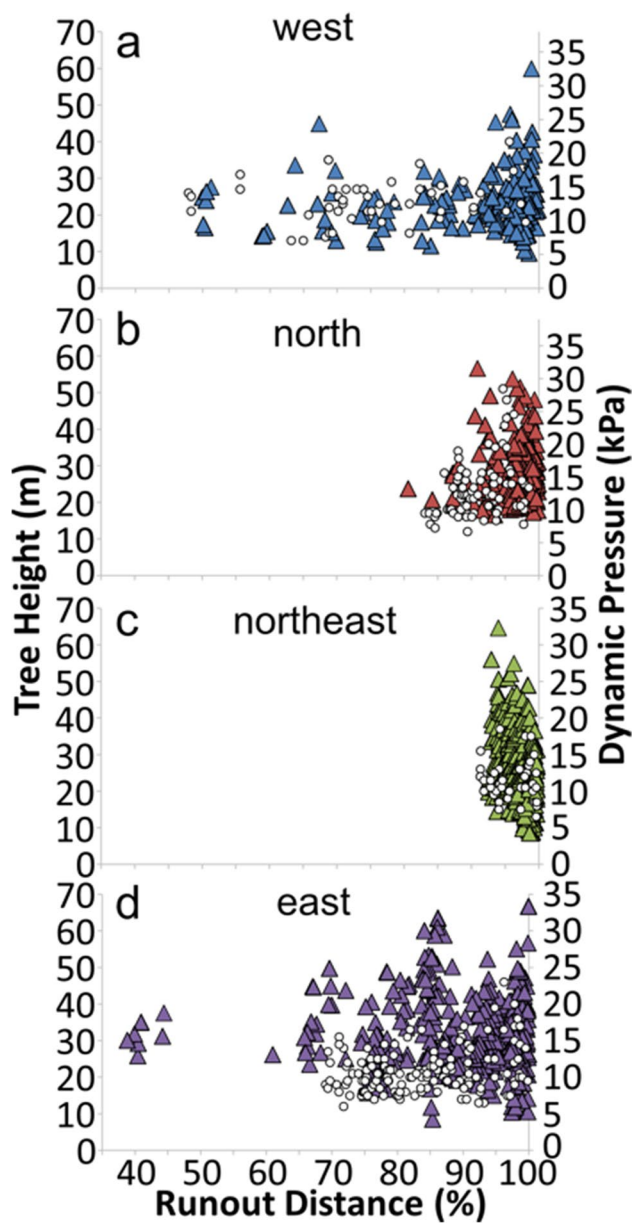


**Fig. 6** Solitary standing tree height and corresponding dynamic pressures as a function of distance towards. **a** West, **b** north, **c** northeast, and **d** east directions of the blowdown zone. Circles represent downed trees; triangles represent standing trees. Colors match flow paths in Fig. 1. Uncertainties are smaller than symbols. Only trees taller than 10 m are included

We recognized and mapped 54 clusters of standing trees in the blowdown zone, 40 newly identified in this study, and 14 out of 51 from Gardner et al. (2018). Standing tree clusters are found on hills that range in height from less than 10 to 417 m, with foreslopes of 5 to 47° (Table 2). When the median aspect of the ground upon which the clusters grew is compared to the bearing of the flow path, 43% of clusters lie on slopes that have aspects that are within  $\pm 30^\circ$  of the cluster flow path, and 68% are within  $\pm 60^\circ$  (Online

**Table 1** Tree height and length statistics for standing and felled solitary trees in the blowdown zone

|           | Standing trees        |             |             | Fallen trees          |             |             |
|-----------|-----------------------|-------------|-------------|-----------------------|-------------|-------------|
|           | Average $\pm$ std (m) | Minimum (m) | Maximum (m) | Average $\pm$ std (m) | Minimum (m) | Maximum (m) |
| West      | 23 $\pm$ 8            | 10          | 60          | 24 $\pm$ 6            | 13          | 40          |
| North     | 28 $\pm$ 7            | 17          | 57          | 24 $\pm$ 8            | 12          | 51          |
| Northeast | 27 $\pm$ 10           | 9           | 65          | 22 $\pm$ 6            | 13          | 37          |
| East      | 31 $\pm$ 9            | 9           | 67          | 22 $\pm$ 6            | 12          | 46          |

**Table 2** Minimum, maximum, and median values of reported attributes by cluster type

|                             | Stripped clusters |            |            | Foliage clusters |            |            |
|-----------------------------|-------------------|------------|------------|------------------|------------|------------|
|                             | Minimum           | Maximum    | Median     | Minimum          | Maximum    | Median     |
| Area (m <sup>2</sup> )      | 16,543            | 133,350    | 72,107     | 3698             | 436,079    | 38,298     |
| Average tree height (m)     | 13 $\pm$ 8        | 40 $\pm$ 8 | 17 $\pm$ 8 | 10 $\pm$ 6       | 36 $\pm$ 6 | 13 $\pm$ 6 |
| Hill height (m)             | 20                | 147        | 46         | 8                | 417        | 49         |
| Hill foreslope (°)          | 13                | 47         | 22         | 5                | 47         | 15         |
| Upstream hill height (m)    | 10                | 250        | 53         | 10               | 259        | 66         |
| Upstream hill foreslope (°) | 5                 | 56         | 19         | 3                | 50         | 16         |

Resource 4). Aspect, the azimuth of the normal to the sloping ground within a pixel, or more simply, the direction a hillslope faces, is determined from the aspect raster within a tree cluster polygon.

Trees in 38 of the standing tree clusters retained their foliage (Fig. 2b); we refer to these as foliage clusters (Fig. 3). The other 14 clusters consist of trees stripped of foliage, referred to as stripped clusters. Most stripped clusters are found to the east and west of the volcano, first appearing at around 40% of runout and persisting to the edge of the blowdown zone (Fig. 1a). The areas of the stripped clusters range from 6000 to 133,400 m<sup>2</sup>. The average height of trees in individual stripped clusters ranges from 13  $\pm$  8 to 40  $\pm$  8 m (Table 2). Nearly half of all hills along flow paths upstream of stripped clusters are taller than those with clusters, having an average height of 57  $\pm$  52 m and an average foreslope of 18  $\pm$  11° (Online Resource 3).

Foliage clusters occur only beyond 70% of the runout distance in all directions (Fig. 1). These tend to cover greater areas than the stripped clusters, ranging from 3698 to 436,100 m<sup>2</sup> (Table 2). Trees within foliage clusters range in height, on average, from 10  $\pm$  6 m to 36  $\pm$  6 m (Table 2). Hills along flow paths upstream of foliage clusters are on average 76  $\pm$  62 m in height, with an average foreslope of 18  $\pm$  10° (Online Resource 3). Two-thirds of hills on flow paths upstream of the foliage clusters are taller than the hill with the foliage cluster.

The PDC traveled past stripped tree clusters at 48–226 m/s and at 47–179 m/s past foliage clusters (Fig. 1a). The velocity of the PDC along flow paths related to solitary standing trees is very similar to that of nearby clusters. Northern areas contain the highest velocities, between 120

and 80 m/s, whereas the east and west have velocities as low as 50 and 60 m/s (Fig. 1a). Note that these velocities are for the frontal edge of the PDC head (Moore and Rice 1984).

### Quantifying $P_{dyn}$ from tree damage

The dynamic pressure ( $P_{dyn}$ ) required to topple a tree of a given size can be estimated from the following, assuming that the tree is cylindrical in shape:

$$P_{dyn} = \frac{\pi r^2 \sigma_{ult}}{4z^2 C_d} \quad (6)$$

where  $r$  is the tree trunk radius,  $\sigma_{ult}$  is the maximum stress at the height of failure, and  $C_d$  is the aerodynamic drag coefficient (Clarke and Voight 2000).  $C_d$  is assumed to equal 1.1 (Rae and Pope 1984; Anderson 1991; Panton 1996; Clarke and Voight 2000). Within the blowdown zone, the majority of trees were Douglas fir and western hemlock (Rosenfeld 1980; Hoblitt et al. 1981; Moore and Sisson 1981; Snellgrove et al. 1983). The average tensile strength for such trees is  $\sigma_{ult} = 63,800 \pm 800$  kPa (Langum et al. 2009). Tree radius ( $r$ ) cannot be accurately resolved in the aerial photographs. Instead, we estimate  $r$  from our measured tree heights, using a relationship derived from data of McPherson et al. (2016). Specifically, McPherson et al. (2016) collected height and diameter at breast height (DBH) for more than 14,000 trees of 171 different species across the USA. From these data, we selected 995 trees in the state of Washington (the same as Mount St. Helens) and found that tree height and DBH correlate strongly (Fig. 7).

Using the DBH/height relationship to find  $r$ , we computed  $P_{dyn}$  for all trees (Fig. 6). Felled trees were assumed to have snapped at their base because pictures available after the disaster support the assumption that most trees were broken near their base. The uncertainty of DBH is 0.11 m and comes from the average residual between the measured Washington trees and modeled DBH. The uncertainty of  $P_{dyn}$  is  $\pm 0.3$  kPa, resulting mainly from the 5-m uncertainty of shadow-derived tree height and the uncertainty associated with  $\sigma_{ult}$ . Standing trees within tree clusters indicate the average  $P_{dyn}$  ( $P_{dyn}^{cluster}$ ) for each cluster ranged from 3 to 23 kPa (Online Resource 5). Therefore, the  $P_{dyn}$  of the PDC impacting the clusters was less than this range since these trees are still standing. The average  $P_{dyn}^{cluster}$  estimated this way does not differ between stripped and foliage clusters nor vary significantly with distance. But,  $P_{dyn}^{cluster}$  is less than  $P_{dyn}$  estimated from nearby solitary standing trees by, on average,  $12 \pm 4$  kPa.

The value for  $P_{dyn}$  estimated from a solitary standing tree can be considered a maximum ( $P_{dyn}^{max}$ ), because that tree was not toppled by the PDC. In contrast,  $P_{dyn}$  estimated from a felled tree can be considered a minimum ( $P_{dyn}^{min}$ ), because it was toppled by the PDC. Ideally, the  $P_{dyn}^{min}$  and  $P_{dyn}^{max}$  would bracket an upper and lower limit for  $P_{dyn}$ , but we find that  $P_{dyn}^{max}$  and  $P_{dyn}^{min}$  range from 10 to 35 and 10 to 32 kPa, respectively, overlapping considerably (Fig. 6). We believe this overlap results from some large trees that were knocked over being either dead or diseased when hit by the PDC and thus weaker than assumed using Eq. (6). It is also possible that some standing trees were shortened by the PDC, which only removed their tops. In addition, smaller trees appear to have been better able to bend rather than break (Fig. 2a; Waitt 1981). Regardless of the overlap, we suggest that overall, the tree damage seen indicates that  $P_{dyn}$  for the PDC was approximately 10–35 kPa over the final ~ 60% of runout.

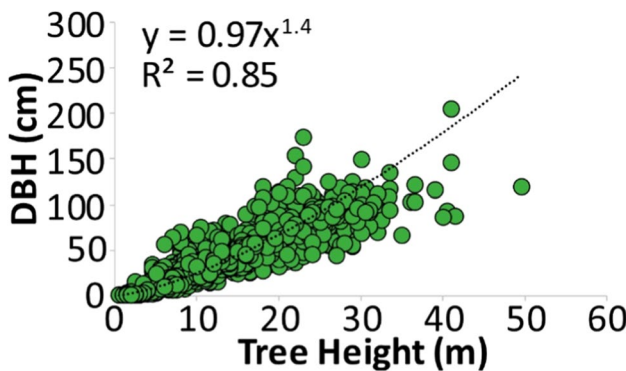


**Fig. 7** Tree height versus tree diameter measured at breast height (DBH; data from McPherson et al. 2016). The best fit ( $R^2=0.85$ ) relationship is  $y=0.97x^{1.4}$

We further posit that  $P_{dyn}$  waned with distance, especially over the final 10% of runout, because (1) standing trees, whether solitary or in clusters, occur only in medial and distal portions of the blowdown zone; (2) the density of standing trees increases markedly with distance (Fig. 5); and (3) trees left standing tend to be taller farther away in most directions from the volcano, reaching ~ 50–60 m at the end of runout (Fig. 6). This result was expected because, in other laterally directed eruptions, less damage is seen in the distal regions because of decreasing flow density and speed, although topography provides some local influences (Belousov et al. 2007). In support, we note that near the source of the PDC,  $P_{dyn}$  is estimated to have been 87–100 kPa (Kieffer 1981; Esposti Ongaro et al. 2011). At 8 km northeast of the volcano (exact location unknown), Clarke and Voight (2000) estimated  $P_{dyn}$  was ~ 40 kPa, based on a toppled 15-m-tall tree ( $r=0.5$  m). At 16 km to the northeast, we estimate  $P_{dyn}^{max} = 34$  kPa and, in the final 20% of runout in the northeast,  $P_{dyn}^{max} = 10$ –30 kPa. We thus conclude that  $P_{dyn}$  of the PDC waned with distance.

Interestingly, our estimate of ~ 10–35 kPa at the edge of the blowdown zone overlaps with the area of 0–35 kPa derived by the model of Esposti Ongaro et al. (2011). We note, however, that trees are damaged to the edge of the blowdown zone, and thus,  $P_{dyn}$  did not decrease to 0 kPa (c.f. Esposti Ongaro et al. 2011). Indeed, velocities derived from the isochrons of the mapped PDC front (Moore and Rice 1984) do not substantially diminish near the edge of the blowdown zone (Fig. 1a). More importantly, Gardner et al. (2017) demonstrated that the PDC did not stop at the end of the blowdown zone, but instead continued into the scorched zone.

### Conceptual model for PDC erupted on 18 May 1980 from Mount St. Helens

Here, we propose a conceptual model for the PDC erupted on 18 May from Mount St. Helens, based on the patterns of tree damage throughout the blowdown zone. Most trees were felled from the impact of the head of the PDC (Rosenbaum and Waitt 1981; Waitt 1981, 2015; Clarke and Voight 2000; Gardner et al. 2017), because  $P_{dyn}$  peaked near the base of the head (Clarke and Voight 2000; Gardner et al. 2017). The PDC head was followed by a relatively slower and denser body (Esposti Ongaro et al. 2012; Gardner et al. 2017). The PDC was also density and velocity stratified. The basal section was slower and denser than the upper section and contained most of the sedimentation processes (Esposti Ongaro et al. 2012; Gardner et al. 2017). Our estimates for  $P_{dyn}$  of the PDC from tree heights are limited to where standing trees are visible in aerial photographs, restricting our model to the outer regions of the blowdown zone. Overall, the

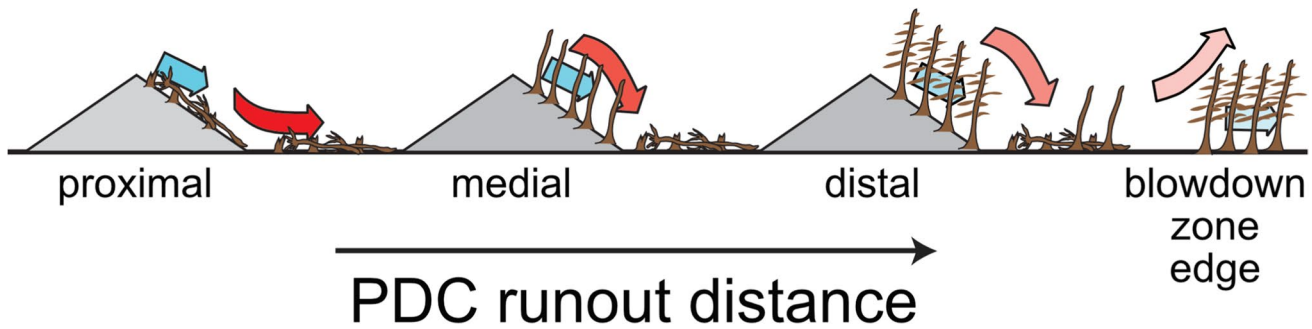


**Fig. 8** Conceptual model of the formation of standing tree clusters on the lee sides of topographic highs. Curved red arrows represent the PDC head; straight blue arrows represent the PDC body. The darker the color, the higher the  $P_{dyn}$ , relatively. At proximal runout distances, the PDC head and body hug topography and the PDC head topples trees. At medial runout distances, the PDC head detaches from the ground and follows a modified path above the lee side of the hill, leaving trees standing but shearing off the treetops. The PDC

body strips these trees of foliage. At distal runout distances, near the edge of the blowdown zone, the PDC head continues to detach and the PDC body flows through lee side clusters but no longer has a dynamic pressure great enough to strip foliage from trees. At the blowdown zone edge, the head of the PDC detaches fully and lifts off, while the PDC body flows into the scorched zone.  $P_{dyn}$  of the PDC body is too low to strip trees of vegetation, but hot enough to damage trees by burning them

number of solitary standing trees and their heights increase with distance in all directions, especially near the end of runout, suggesting that  $P_{dyn}$  of the PDC decreases dramatically in the final stages before liftoff. In addition, standing solitary trees are found over the last 60% of runout towards the east and west, but only in the outer 20% in the north and northeast. That pattern suggests that  $P_{dyn}$  of the PDC was greater towards the north and northeast.

$P_{dyn}$  can vary significantly due to small differences in velocity (Eq. 1). The different spatial patterns of solitary trees left standing across the blowdown zone (Figs. 5 and 6) may thus result from higher velocities of the head of the PDC towards the north and northeast, because the PDC was erupted mainly in that direction (Kieffer and Sturtevant 1988). Indeed, the velocity of the PDC head at the outer edge of the blowdown zone in the north and northeast was  $\sim 80$  m/s, whereas it was 50–60 m/s at the outer edge in the east and west (Fig. 1a; derived from Moore and Rice 1984). In addition, trees were felled by the head of the PDC up until the edge of the blowdown zone. This relationship demonstrates that  $P_{dyn}$  of the PDC did not drop to zero in the blowdown zone as indicated by Esposti Ongaro et al. 2011.  $P_{dyn}$  also depends on flow density (Eq. 1). Gardner et al. (2017) argued that tree clusters were left standing only when the thermal energy of the PDC had decreased enough to not expand downward when it leapt over hills. Loss of thermal energy comes mainly from sedimentation of mass and hence a decrease in flow density (Gardner et al. 2017). It is thus likely that the spatial pattern of standing trees reflects both the velocity of the PDC and sedimentation of mass from it.

Our conceptual model suggests that damage to solitary trees acts as proxy for the evolution of  $P_{dyn}$  of the head of the PDC. We posit that damage to standing tree clusters reflects  $P_{dyn}$  of the body of the PDC (Fig. 7). Gardner

et al. (2018) argued that clusters of standing trees were preserved because the head of the PDC, where the peak  $P_{dyn}$  of the PDC occurred, temporarily rose above the trees as it traversed hill lee sides. In this study, we show that standing trees within clusters are damaged, indicating that trees were impacted by  $P_{dyn}$ . In particular, trees were either stripped of foliage or retained scorched foliage. We suggest that although some hills were able to protect trees on lee sides from the brunt of the head of the PDC, the trailing body of the PDC did not jump over the hill, but instead hugged topography throughout the blowdown zone, running through clusters left standing by the PDC head (Fig. 8).  $P_{dyn}$  of the body was not great enough to topple the standing trees in clusters but was significant enough to strip vegetation from some. Towards the east and west,  $P_{dyn}$  of the body at between  $\sim 40$  and  $\sim 70\%$  of runout was high enough to strip trees of vegetation, but not high enough to topple large trees, leaving behind the stripped clusters. In these stripped clusters, we also posit that the head of the PDC did not lift high enough over the trees and sheared off the treetops. Towards the north and northeast over those same medial distances, however, the  $P_{dyn}$  of the PDC body was too high to leave behind standing trees. After 70% runout in all directions, the  $P_{dyn}$  of the PDC body had decreased enough that tall trees were not stripped of vegetation, but only scorched from the heat, leaving foliage clusters. On average, we estimate  $P_{dyn}$  that impacted tree clusters was  $12 \pm 4$  kPa less than what hit trees not shielded by hills; therefore, the  $P_{dyn}$  of the PDC body was less than the head. Gardner et al. (2018) argued that greater  $P_{dyn}$  in the PDC head resulted from its higher velocities. A denser body lagging behind a faster head agrees with previous numerical and observational studies (Benage et al. 2016; Breard and Lube 2017; Scharff et al. 2019).

## Conclusions

Solitary standing trees and standing trees in 54 clusters were counted and measured in aerial photographs from across the so-called blowdown zone of the forest destroyed by the PDC produced at Mount St. Helens on 18 May 1980. Tree heights and downed tree lengths were used to estimate the dynamic pressure ( $P_{dyn}$ ) exerted by the PDC.  $P_{dyn}$  of the PDC head ranged from 10 to 35 kPa over the final ~60% of runout of the PDC.  $P_{dyn}$  waned with distance, especially in the final 10% of runout, as indicated by the observations that standing trees occur only in the outer ~60% of runout, the density of standing trees increases dramatically with distance, and trees left standing tend to be taller farther away from the volcano. On average,  $P_{dyn}$  of the body of the PDC was  $12 \pm 4$  kPa less than the head at similar distances from the volcano. The body, however, damaged and scorched trees in clusters on lee sides of hills that had protected those trees from the head of the current. It is likely that the body hugged topography because of its slower velocity, which also explains its lower  $P_{dyn}$ . Despite waning  $P_{dyn}$  with distance, the PDC still toppled trees at the distal end of the blowdown zone, and thus,  $P_{dyn}$  did not drop to 0 kPa in the blowdown zone.

**Supplementary Information** The online version contains supplementary material available at <https://doi.org/10.1007/s00445-022-01548-6>.

**Acknowledgements** We thank Laura Pioli, Alvaro Aravena, and an anonymous reviewer for insightful reviews of an earlier version of this manuscript. We also thank Gabrielle Varona and Caroline Nazworth for their assistance with collecting data. The authors acknowledge support from the National Science Foundation from grant EAR-1852449 to JEG, the Department of Geological Sciences Owen-Coats fund, and from the Jackson School of Geoscience.

**Open Access** This article is licensed under a Creative Commons Attribution 4.0 International License, which permits use, sharing, adaptation, distribution and reproduction in any medium or format, as long as you give appropriate credit to the original author(s) and the source, provide a link to the Creative Commons licence, and indicate if changes were made. The images or other third party material in this article are included in the article's Creative Commons licence, unless indicated otherwise in a credit line to the material. If material is not included in the article's Creative Commons licence and your intended use is not permitted by statutory regulation or exceeds the permitted use, you will need to obtain permission directly from the copyright holder. To view a copy of this licence, visit <http://creativecommons.org/licenses/by/4.0/>.

## References

Anderson JD (1991) Fundamentals of aerodynamics. McGraw-Hill, New York

Andrews BJ, Manga M (2012) Experimental study of turbulence, sedimentation, and coignimbrite mass partitioning in dilute pyroclastic density currents. *J Volcanol Geotherm Res* 225–226:30–44

Auker MR, Sparks RSJ, Siebert L, Crosweller HS, Ewert J (2013) A statistical analysis of the global historical volcanic fatalities record. *J Appl Volcanol* 2:2. <https://doi.org/10.1186/2191-5040-2-2>

Baxter PJ (1990) Medical effects of volcanic eruptions. *Bull Volcanol* 52:532–544. <https://doi.org/10.1007/BF00301534>

Baxter PJ, Neri A, Todesco M (1998) Physical modelling and human survival in pyroclastic flows. *Nat Hazards* 17:163–176

Baxter PJ, Boyle R, Cole P, Neri A, Spence R, Zuccaro G (2005) The impacts of pyroclastic surges on buildings at the eruption of the Sourfrière Hills volcano, Montserrat. *Bull Volcanol* 67:292–313. <https://doi.org/10.1007/s00445-004-0365-7>

Baxter PJ, Jenkins S, Seswandhana R, Komorowski JC, Dunn K, Purser D, Voight B, Shelley I (2017) Human survival in volcanic eruptions: thermal injuries in pyroclastic surges, their causes, prognosis and emergency management. *Burns* 43:1051–1069. <https://doi.org/10.1016/j.burns.2017.01.025>

Benage MC, Dufek J, Mothes PA (2016) Quantifying entrainment in pyroclastic density currents from the Tungurahua eruption, Ecuador: integrating field proxies with numerical simulations. *Geophys Res Lett* 43:6932–6941. <https://doi.org/10.1002/2016GL069527>

Blong RJ (1984) Volcanic hazards: a sourcebook on the effects of eruptions. Academic, Sydney, p 424

Brand BD, Gravley DM, Clarke AB, Lindsay JM, Bloomberg SH, Agustin-Flores J, Németh K (2014) A combined field and numerical approach to understanding dilute pyroclastic density current dynamics and hazard potential: Auckland volcanic field, New Zealand. *J Volcanol Geotherm Res* 276:215–232. <https://doi.org/10.1016/j.volgeores.2014.01.008>

Branney MJ, Kokelaar P (2002) Pyroclastic density currents and the sedimentation of ignimbrites. The Geological Society, London, Memoir No, p 27

Breard ECP, Lube G (2017) Inside pyroclastic density currents – uncovering the enigmatic flow structure and transport behavior in large-scale experiments. *Earth Planet Sci Lett* 458:22–36. <https://doi.org/10.1016/j.epsl.2016.10.016>

Christiansen RL, Peterson DW (1981) Chronology of the 1980 eruptive activity. In Lipman PW, Mullineaux DR. (eds) The 1980 eruptions of Mount St. Helens, Washington. US Geol Surv Prof Pap 1250:17–30.

Clarke AB, Voight B (2000) Pyroclastic current dynamic pressure from aerodynamics of tree or pole blow-down. *J Volcanol Geotherm Res* 100:395–412. [https://doi.org/10.1016/S0377-0273\(00\)00148-7](https://doi.org/10.1016/S0377-0273(00)00148-7)

Doronzio DM, de Tullio MD, Dellino P, Pascazio G (2011) Numerical simulation of pyroclastic density currents using locally refined Cartesian grids. *Comput Fluids* 56–67. <https://doi.org/10.1016/j.compfluid.2010.12.006>

Druitt TH (1998) Pyroclastic density currents. Geological Society, London Special Publications 45:145–182. <https://doi.org/10.1144/GSL.SP.1996.145.01.08>

Dufek J, Esposti Ongaro T, Roche O (2015) Pyroclastic density currents: processes and models. The Encyclopedia of Volcanoes (second Edition) 617–629. <https://doi.org/10.1016/B978-0-12-385938-9.00035-3>

Esposti Ongaro T, Neri A, Todesco M, Macedonio G (2002) Pyroclastic flow hazard assessment at Vesuvius (Italy) by using numerical modeling. II. Analysis of Flow Variables *Bull Volcanol* 64:178–191. <https://doi.org/10.1007/s00445-001-0190-1>

Esposti Ongaro T, Widiwijayanti C, Clarke AB, Voight B, Neri A (2011) Multiphase-flow numerical modeling of the 18 May 1980 lateral blast at Mount St. Helens, USA. *Geology* 39:535–538. <https://doi.org/10.1130/G31865.1>

Esposti Ongaro T, Clarke AB, Voight B, Neri A, Widiwijayanti C (2012) Multiphase flow dynamics of pyroclastic density currents

during the May 18, 1980 lateral blast of Mount St. Helens. *J Geophys Res* 117:B06208. <https://doi.org/10.1029/2011JB009081>

Gardner JE, Andrews BJ, Dennen R (2017) Liftoff of the 18 May 1980 surge of Mount St. Helens (USA) and the deposits left behind. *Bull Volcanol* 79:8. <https://doi.org/10.1007/s00445-016-1095-3>

Gardner JE, Nazworth C, Helper MA, Andrews BJ (2018) Inferring the nature of pyroclastic density currents from tree damage: the 18 May 1980 blast surge of Mount St. Helens, USA. *Geology* 46(9):795–798. <https://doi.org/10.1130/G45353.1>

Hoblitt RP, Miller CD, Vallance JW (1981) Origin and stratigraphy of the deposit produced by the May 18 directed blast. In Lipman PW, Mullineaux DR. (eds) The 1980 eruptions of Mount St. Helens, Washington. US Geol Surv Prof Pap 1250:401–420.

Hoblitt RP (2000) Was the 18 May 1980 lateral blast at Mt St Helens the product of two explosions? *Phil Trans R Soc Lond A* 358:1639–1661

Iangum CE, Yadama V, Iowell EC (2009) Physical and mechanical properties of young-growth Douglas-fir and western hemlock from western Washington. *Forest Prod J* 59:37–47

Jenkins S, Komorowski JC, Baxter PJ, Spence R, Picquout A, Lavigne F, Surono (2013) The Merapi 2010 eruption: an interdisciplinary impact assessment methodology for studying pyroclastic density current dynamics. *J Volcanol Geotherm Res* 261:316–329. <https://doi.org/10.1016/j.volgeores.2013.02.012>

Kelfoun K, Legos F, Gourgaud A (2000) A statistical study of trees damaged by the 22 November 1994 eruption at Merapi volcano (Java, Indonesia): relationships between ash-cloud surges and block-and-ash flows. *J Volcanol Geotherm Res* 100:379–393. [https://doi.org/10.1016/S0377-0273\(00\)00147-5](https://doi.org/10.1016/S0377-0273(00)00147-5)

Kieffer SW (1981) Fluid dynamics of the May 18 blast at Mount St. Helens. In Lipman PW, Mullineaux DR (eds) The 1980 eruptions of Mount St. Helens, Washington. US Geol Surv Prof Pap 1250:379–400.

Kieffer SW, Sturtevant B (1988) Erosional furrows formed during the lateral blast at Mount St. Helens, May 18, 1980. *J Geophys Res* 93:14793–14816

Lipman PW, Mullineaux DR. (eds) (1981) The 1980 eruptions of Mount St. Helens, Washington. US Geol Surv Prof Pap 1250.

McPherson GE, van Doorn NS, Peper PJ (2016) Urban tree database, Fort Collins, CO. Forest Service Research Data Archive. Updated 21 January 2020. <https://doi.org/10.2737/RDS-2016-0005>

Moore JG, Rice C (1984) Chronology and character of the May 18, 1980 explosive eruption of Mount St. Helens. In, *Explosive volcanism: inception, evolution and hazards*. Wash D.C., Nat Acad Press 133–142.

Moore JG, Sisson TW (1981) Deposits and effects of the May 18 pyroclastic surge. In Lipman PW, Mullineaux DR. (eds) The 1980 Eruptions of Mount St. Helens, Washington. US Geol Surv Prof Pap 1250:53–6.

Panton RL (1996) Incompressible Flow. Wiley, New York

Pitarri A, Cas RAF, Monaghan JJ, Martí J (2007) Instantaneous dynamic pressure effects on the behavior of lithic boulders in pyroclastic flows: the Abrigo Ignimbrite, Tenerife, Canary Islands. *Bull Volcanol* 69:265–279. <https://doi.org/10.1007/s00445-006-0072-7>

Rae WH, Pope A (1984) Low-speed wind tunnel testing. Wiley, New York

Roche O, Niño Y, Mangeney A, Brand B, Pollock N, Valentine GA (2013) Dynamic pore-pressure variations induce substrate erosion by pyroclastic flows. *Geology* 41:1107–1110. <https://doi.org/10.1130/G34668.1>

Rosenbaum JG, Waitt RB (1981) Summary of eyewitness account of the May 18 eruption. In Lipman PW, Mullineaux DR. (eds) The 1980 eruptions of Mount St. Helens, Washington. US Geol Surv Prof Pap 1250:53–68.

Rosenfeld CL (1980) Observations of the Mount St. Helens Eruption. *Am Sci* 68:494–509

Scharff L, Hort M, Varley NR (2019) First in-situ observation of a moving natural pyroclastic density current using Doppler radar. *Sci Rep* 9:7386. <https://doi.org/10.1038/s41598-019-43620-w>

Snellgrove TA, Kendall Snell JA, Max TA (1983) Damage to National Forest timber on Mount St. Helens. *J Forest* 81:368–371

Tilling RI, Swanson TL, Swanson DA (1990) Eruptions of Mount St. Helens: past, present, and future. US Geol Surv Spec Int Pub 56. [https://web.archive.org/web/20111026174423/http://vulcan.wr.usgs.gov/Volcanoes/MSH/Publications/MSHPPF/MSH\\_past\\_present\\_future.html](https://web.archive.org/web/20111026174423/http://vulcan.wr.usgs.gov/Volcanoes/MSH/Publications/MSHPPF/MSH_past_present_future.html)

Valentine GA (1998) Damage to structures by pyroclastic flows and surges, inferred from nuclear weapons effects. *J Volcanol Geotherm Res* 87:117–140. [https://doi.org/10.1016/0377-0273\(86\)90026-0](https://doi.org/10.1016/0377-0273(86)90026-0)

Waitt RB (1981) Devastating pyroclastic density flow and attendant air fall of May 18 – stratigraphy and sedimentology of deposits. In Lipman PW, Mullineaux DR. (eds) The 1980 eruptions of Mount St. Helens, Washington. US Geol Surv Prof Pap 1250:439–458.

Waitt RB (2015) In the path of destruction: eyewitness chronicles of Mount St. Helens. WSU Pr Pullman WA.